Sturala et al. *NPG Asia Materials* (2019) 11:42
https://doi.org/10.1038/s41427-019-0142-x

NPG Asia Materials

ARTICLE Open Access

Coordination chemistry of 2D and layered gray arsenic: photochemical functionalization with chromium hexacarbonyl

Jiri Sturala[1], Zdenek Sofer[1] and Martin Pumera[1,2,3]

Abstract

The functionalization of layered materials is one of the current challenges in material science. Exfoliated rhombohedral (gray) arsenic represents a promising layered material for the fabrication of electronic devices and sensors; however, synthetic protocols for tuning its properties or protecting the surface by covalent functionalization are not known. In this communication, we present its covalent functionalization accompanied by the exfoliation of rhombohedral arsenic in the presence of ultraviolet light irradiation and chromium hexacarbonyl. During this modification, the arsenic atoms act as ligands to the chromium metal center. We believe that this study provides a promising approach for the modification of rhombohedral few-layer arsenene and enables its application in various fields, including electronic devices, sensors, and energy devices.

Introduction

Two-dimensional layered materials are topics of interest in material science because they bear unique properties that are often not observed in bulk materials[1–4]. Among them, layered materials composed of monoelemental sheets from the 15th group of elements (pnictogens) are considered to be materials beyond graphene that can overcome or improve its properties, e.g., they have a direct bandgap in a single/few-layered form. On the other hand, the chemistry of layered pnictogens is almost unexplored, which is the key to the surface protection and tuning of its properties. Most chemical functionalization has been performed on layered black phosphorus. The derivatization of pnictogens is divided into two main approaches—noncovalent and covalent functionalization. Noncovalent functionalization is based on the interaction of pnictogen lone pairs with electron-deficient systems, e.g., 7,7,8,8-tetracyano-*p*-quinodimethane[5], large polyaromatic systems based on perylenes[6], fullerenes[7], or tetracyanoethylene[8]. Interestingly, black phosphorus can also interact with electron-rich systems, e.g., tetrathiafulvalenes[8]. The second major type of noncovalent functionalization is mediated by the interaction of the surface with solvents, ionic liquids[9], and surfactants[10,11], which protect the surface and make the exfoliation easier. Antimonene was also functionalized by a similar approach as black phosphorus, which involved an interaction with perylene-based electron-acceptors[12] and polyethylene glycol[13] and arsenene with anthraquinone[14]. Covalent modifications are scarce and are limited exclusively to black phosphorus. Among them, the most important are modifications based on diazonium salt chemistry[15–17], which introduce functionalities for tuning the properties or protecting the surface toward oxidation, which is an another important issue in pnictogen chemistry or for enabling another modification.

Correspondence: Zdenek Sofer (zdenek.sofer@vscht.cz) or Martin Pumera (pumera.research@gmail.com)
[1]Department of Inorganic Chemistry, University of Chemistry and Technology Prague, Technicka 5, 166 28 Prague 6, Czech Republic
[2]Department of Chemical and Biomolecular Engineering, Yonsei University, 50 Yonsei-ro, Seodaemun-gu, Seoul 03722, Korea
Full list of author information is available at the end of the article.

Experimental methods

Material preparation

The gray arsenic (150 mg, 2 mmol) was finely grounded under an argon atmosphere and dispersed in dry deoxygenated acetonitrile (150 mL). Chromium hexacarbonyl (44 or 662 mg; 0.2 or 3 mmol, respectively) was added, and the mixture was irradiated with a high-pressure mercury lamp for 30 min without cooling. After ~10 min, the solvent reached the boiling point, which was beneficial for carbon monoxide elimination from the reaction mixture. After cooling to room temperature, the mixture was filtered in a glovebox under an argon inert atmosphere, washed with dry deoxygenated acetonitrile and dichloromethane, and the product was dried in vacuo.

The control experiment was performed under the same conditions (gray As (150 mg, 2 mmol), chromium hexacarbonyl (44 mg, 0.2 mmol)) in boiling deoxygenated acetonitrile (150 mL) under an argon atmosphere for 30 min in the dark.

Fourier transform infrared (FTIR) spectroscopy

FTIR spectroscopy measurements were performed on an iS50R FTIR spectrometer (Thermo Scientific, USA). The measurement was performed using a DLaTGS detector and a KBr beam splitter in the range of 4000–400 cm^{-1} at a resolution of 4 cm^{-1}. The samples were measured using KBr pellets made from 300 mg finely grounded KBr and 1 mg of the sample.

Raman spectroscopy

An inVia Raman microscope (Renishaw, England) in backscattering geometry with a CCD detector was used for Raman spectroscopy. A DPSS Nd-YAG laser (532 nm, 50 mW) with an applied power of 0.5% and a ×50 magnification objective were used. The spectra were referenced according to a laser peak at 0 cm^{-1}, and the spectrometer was calibrated prior to the measurements by acquiring a spectrum of silicon and referenced it to 521 cm^{-1}. The samples were deposited on a metal plate as a powder and measured immediately after deposition.

X-ray photoelectron spectroscopy (XPS)

High-resolution XPS was performed using an ESCA-ProbeP spectrometer (Omicron Nanotechnology Ltd, Germany) with a monochromatic aluminum X-ray radiation source (1486.7 eV). Wide-scan surveys of all elements were performed, with subsequent high-resolution scans of the C 1 s, As 3p or As 3d, Cr 2p, and O 1 s. Relative sensitivity factors were used to evaluate the element ratios from the survey spectra. The samples were placed on a conductive carrier made from a high-purity silver or bar. An electron gun was used to eliminate sample charging during measurement (1–5 V). The values were referenced to the gold peak at 84.0 eV or adventitious carbon peak at 284.8 eV.

High-resolution transmission electron microscopy (HR-TEM)

HR-TEM was performed using an EFTEM 2200 FS microscope (JEOL, Japan). A 200 keV acceleration voltage was used for measurement. Elemental maps and EDS spectra were acquired with an SDD detector X-MaxN 80 TS from Oxford Instruments (England). Samples were prepared by drop casting the suspension (1 mg mL^{-1} in water) on a TEM grid (Cu, 200 mesh, Formvar/carbon) and drying them at 60 °C for 12 h.

DFT calculations

The cell containing an arsenic monolayer with 18 arsenic atoms and a $Cr(CO)_3$ moiety in the center or four $Cr(CO)_6$ clusters was optimized using Quantum Espresso code[18] to a minimum using PBE DFT functional and PAW pseudopotentials. The IR spectrum was then calculated using the Phonon package from Quantum Espresso code. The resulting IR spectra were not scaled.

Results and discussion

In this communication, we present a conceptually new approach of covalent functionalization of gray arsenic with chromium hexacarbonyl, where arsenic atoms play a role in ligands of the chromium metal center under photochemically facilitated conditions. A similar interaction of phosphorus with metal carbonyls in homogeneous systems is well documented in the literature[19] and was also reported for carbon materials (graphene[20] and nanotubes[21]), which mimic metal aromatic complexes, e.g., bis(benzene)chromium.

The gray arsenic used for the modification was pulverized in an agate mortar under an argon inert atmosphere to prevent surface oxidation and immediately added into deoxygenated anhydrous acetonitrile containing chromium (0) hexacarbonyl. The reaction mixture was irradiated by a high-pressure mercury lamp in a quartz flask. Under such conditions[22], the metal carbonyls lost carbon monoxide (Scheme 1a), and the empty orbital was filled with another ligand, such as a solvent molecule or another donor, which was an arsenic atom in this case (Scheme 1b). The structure of gray arsenic has an arrangement that can replace up to three CO groups; according to FTIR and TG-MS analysis (see corresponding sections), therefore, the main product of the reaction is the structure with the simplified formula $As_3Cr(CO)_3$. However, species with only two or one replaced CO ligands were also detected. In addition, some of the carbonyls in the product can be replaced with acetonitrile, forming more complex products with the general formula $As_xCr(CO)_{6-x-y}(MeCN)_y$, where "$x$" is in the range of 1–3 and "y" is in the range of 0–3. The major product,

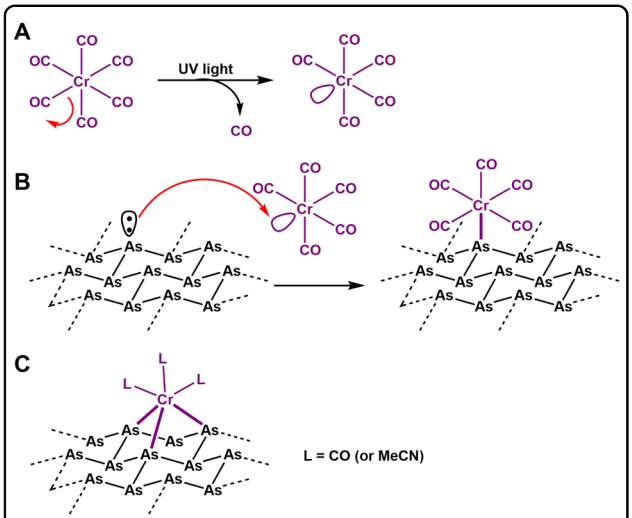

Scheme 1 Simplified mechanism showing **a** the formation of coordinative unsaturated reactive $Cr(CO)_5$ species, **b** its reaction with an arsenic lone pair and formation of $As_1Cr(CO)_5$ product, and **c** the final product with three ligands replaced by three arsenic lone pairs

$As_3Cr(CO)_3$ (Scheme 1c), was formed due to the proximity effect of other arsenic atoms, which were prearranged in the correct positions; therefore, the loss of the second and third carbon monoxide and the formation of high-level complexes was easier than in the first step.

To confirm the functionalization of the layered gray arsenic, the following sets of characterizations were performed. Via HR-TEM/EDS analysis, a uniform distribution of arsenic, chromium, carbon, and oxygen was observed and supports the idea that the chromium carbonyl moiety was bound to the arsenic surface. In addition, the process was accompanied by further changes in the morphology of the arsenic, showing that defects formed during functionalization, as indicated by the HR-TEM/EDS images (Fig. 1). The HR-TEM images are shown for the product modified with 1.5 eq. of $Cr(CO)_6$. For other samples, see Supplementary Figs. S1 and S2. Additional images of the arsenic sheet obtained by TEM are shown in the Supporting Information (Fig. S3). The morphology was further studied by atomic force microscopy (AFM). The individual typical flakes typically had lateral sizes that reached ~1 μm with a thickness of 10 to approximately 150 nm. The AFM images are shown in Supplementary Fig. S4.

The presence of CO ligands was easily proven by FTIR spectroscopy because the vibrational frequency of CO groups for metal carbonyls is characteristic and depends on the type and number of other ligands[23]. To prove our hypothesis that ultraviolet (UV) irradiation is beneficial, we performed a control experiment under the same conditions without UV irradiation, but the CO vibrational band was not observed. This is in accordance with the proposed mechanism in which metal carbonyls are excited to a high energetic state after irradiation where one CO group is detached (which is also supported by the solvent at the boiling point by removing CO from the proximity of the metal complex). The formed unsaturated complex is relatively stable and can interact with the arsenic lone pair. A simple thermal activation at the acetonitrile boiling point temperature (82 °C) was not sufficient to replace the CO ligand(s) with arsenic. The main vibrational band was observed at 1934 cm^{-1} for the main product if 0.1 or 1.5 eq. of $Cr(CO)_6$ were used, which is clearly different from the starting $Cr(CO)_6$ complex with a CO vibration of 1992 cm^{-1}. This observation supports the formation of donor–acceptor bonds between the arsenic and chromium centers. We assumed that the use of 0.1 eq. of $Cr(CO)_6$ created sufficiently diluted solution, therefore, the less substituted chromium carbonyls with a simplified formula of $As_{1-2}Cr(CO)_{4-5}$ were not formed at a significant amount due to the proximity effect mentioned previously. In contrast, 1.5 eq. of $Cr(CO)_6$ saturated the surface more effectively than 0.1 eq., and a small amount of less substituted complexes were formed with vibrational bands at 2054 and 2015 cm^{-1}. The peak at 2203 cm^{-1} was assigned as a CN group from acetonitrile, which also replaced some CO ligands in the product (Fig. 2). In addition, the products were not contaminated with the oxidation product As_2O_3 at high concentrations, as is evident from the FTIR spectra. The gray arsenic contained some As_2O_3 on the surface; however, most of the oxide was formed during the preparation of KBr pellets where exposure to the air could not be avoided. According to the DFT calculation, the shift toward low wavenumbers supports the substitution of CO ligands by arsenic atoms in the products (for theoretical IR spectra, see Supplementary Fig. S5). Raman spectra of the functionalized arsenic show significant broadening of both the phonon mode E_g (195 cm^{-1}) and A_{1g} (257 cm^{-1}) in comparison with the bulk. A similar effect was observed on a few-layered arsenenes obtained by InAs plasma-assisted decomposition[24]. Interestingly, arsenic oxide can be detected only in the starting arsenic and arsenic samples reacted without UV exposure. The results of Raman spectroscopy are shown in Supplementary Fig. S6.

Carbonyl complexes are generally thermally unstable and decompose to gaseous products, which correspond to the attached ligands[25]. The TG-MS analysis confirmed that carbon monoxide was released from the sample at temperatures exceeding 100 °C with two main maxima at 152 and 195 °C and a third one at ~345 °C. The acetonitrile was released from the sample at 250 °C, reaching maximum at 355 °C (Fig. 3).

The surface modification and the elemental composition of gray arsenic with chromium hexacarbonyl were further studied by XPS. The elemental composition is summarized in Table 1, and the survey spectrum of gray

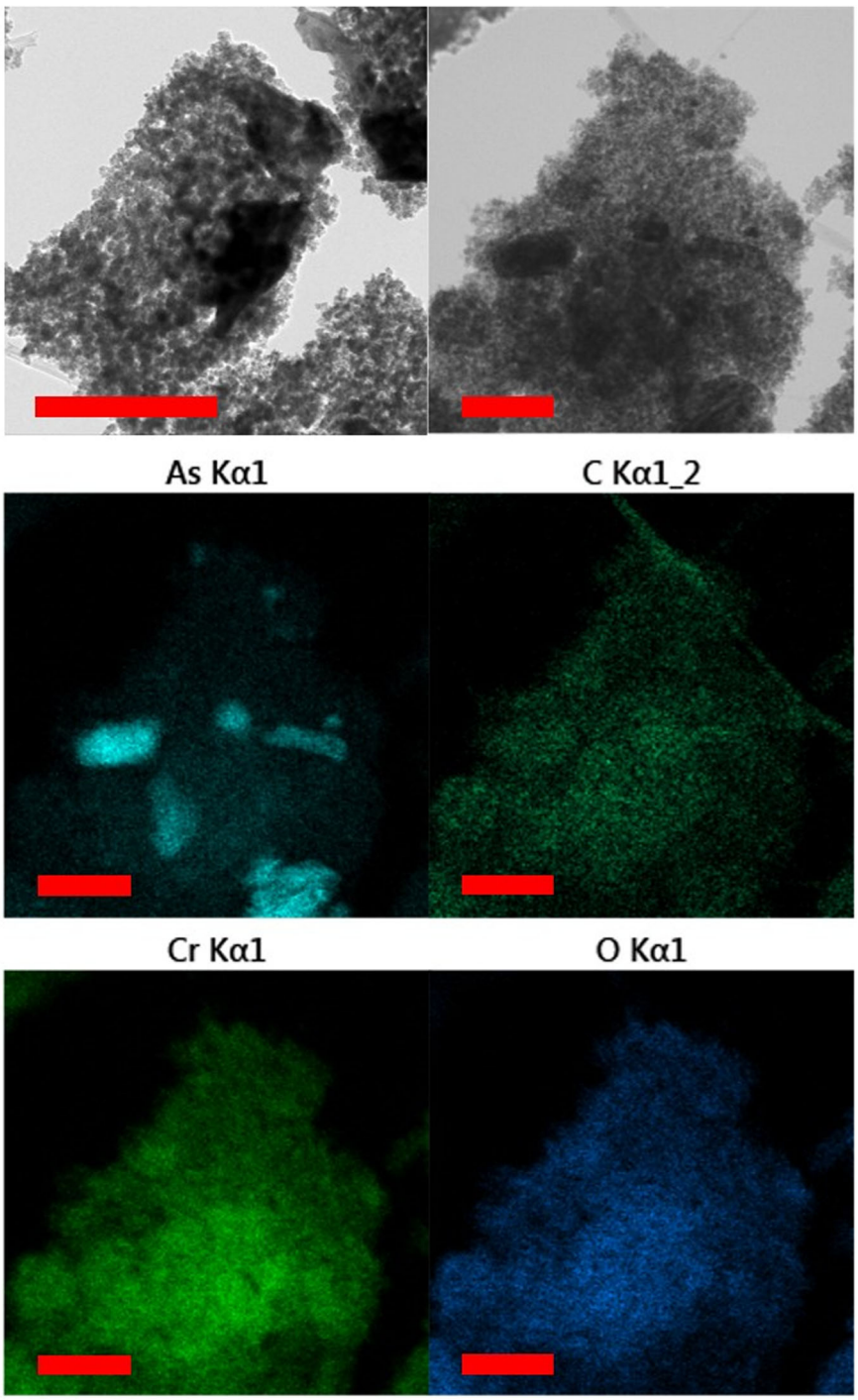

Fig. 1 HR-TEM/EDX images of $Cr(CO)_6$ modified arsenic and elemental distribution maps of As, Cr, C, and O. Scale bars are 1 μm

arsenic modified with 1.5 eq. of $Cr(CO)_6$ is shown in Fig. 4a. For the other samples, see Supplementary Figs. S8–S10. The gray arsenic sample modified with 1.5 eq. of $Cr(CO)_6$ showed two peaks in the arsenic $3p_{3/2}$ region (the 3d region is usually the main region of interest for As but cannot be used because the peaks overlap with the Cr 3p peaks). The peaks at 142.6 and 144.4 eV correspond to $3p_{3/2}$ peaks of arsenic–chromium complexes with the general formulas of As_3CrL_3 and As_2CrL_4, respectively (Fig. 4b), where L is used for the general ligand; however, the main ligand is CO. The formation of the complex is also supported by the chromium $2p_{3/2}$ peak at 575.6 eV.

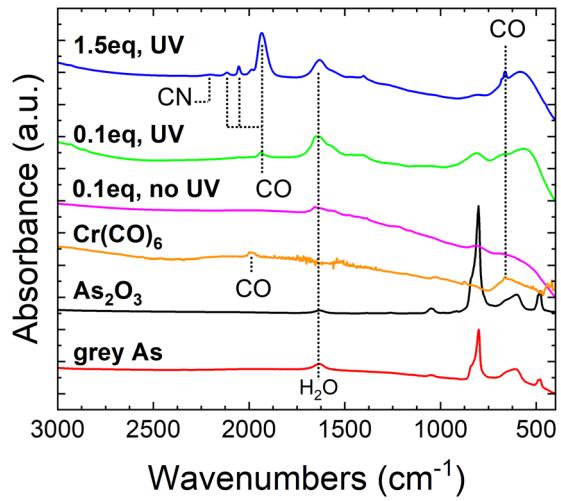

Fig. 2 FTIR spectrum in the KBr pellet of gray arsenic (red), possible oxidation product As_2O_3 (black), $Cr(CO)_6$ (orange), control experiment without UV irradiation (magenta), and modified arsenic with 0.1 eq. (green) and 1.5 eq. (blue) of $Cr(CO)_6$

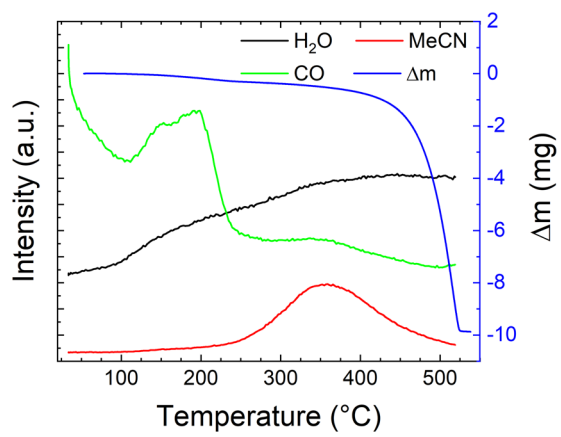

Fig. 3 Thermogravimetric data for $Cr(CO)_6$ (1.5 eq.)-modified arsenic showing the mass difference (blue) and curves corresponding to release of water (black), carbon monoxide (green), and acetonitrile (red) as a function of the temperature

Table 1 Elemental composition of $Cr(CO)_6$ modified gray arsenic samples

Sample	As [at%]	Cr [at%]	C [at%]	N [at%]	O [at%]
1.5 eq., UV	10.4	10.0	39.9	1.6	38.1
0.1 eq., UV	9.5	11.0	36.8	–[a]	42.8
0.1 eq., no UV	69.4	–[a]	18.7	–[a]	12.0
Gray As (blank)	68.8	–[a]	17.5	–[a]	13.7

[a]Not detected in significant amount

The second peak at 577.6 eV corresponds to Cr^{3+} oxide, which was formed during the manipulation with the sample before the measurement and protected the arsenic surface (Fig. 4c). However, the presence of Cr_2O_3 in the

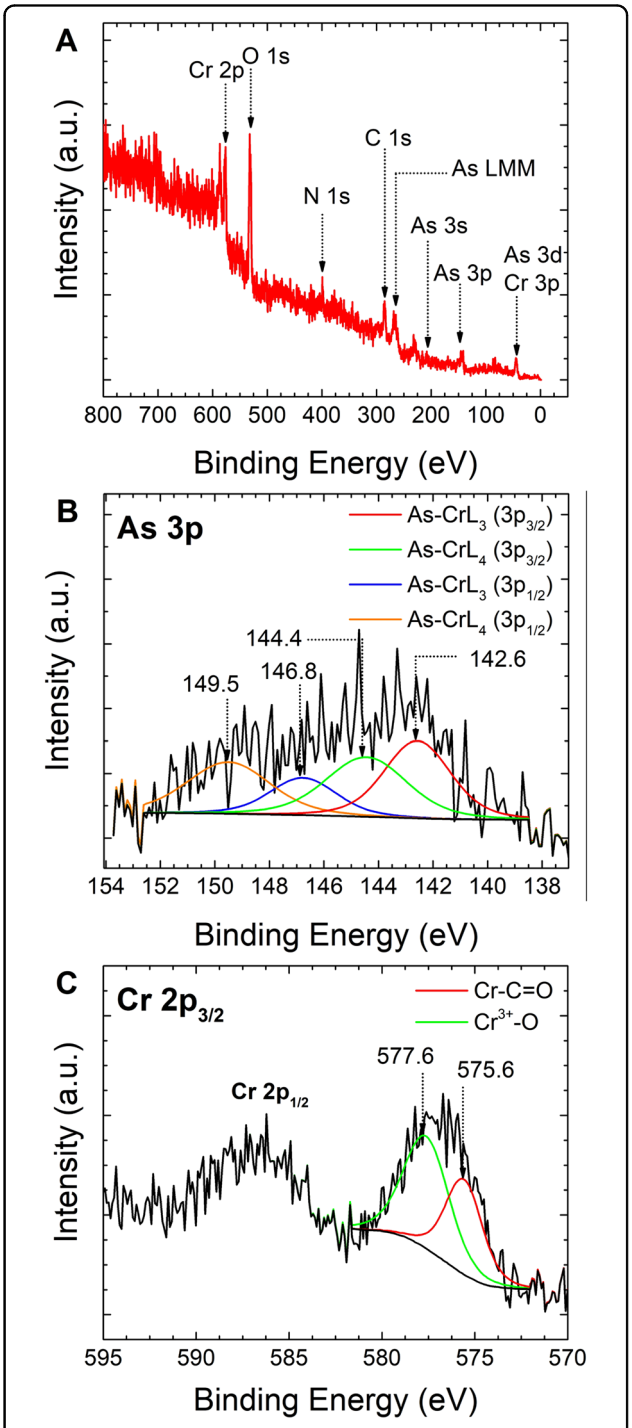

Fig. 4 a The survey spectrum of 1.5 eq. $Cr(CO)_6$-modified gray arsenic and high-resolution XPS spectra. **b** As 3p and **c** Cr 2p. L represents ligand (majority is L = CO), dashed magenta line is the envelope expressed as a sum of individual fitted components

Table 2 Selected As and Cr XPS peaks of prepared materials

Entry	Sample	As $3p_{3/2}$	As $3d_{5/2}$	Cr $2p_{3/2}$	Ratio of As $3p_{3/2}$ peaks
1	1.5 eq., UV	142.6 144.4	–[a]	575.6	1:1
2	0.1 eq., UV	143.2 145.1	–[a]	575.6	5:1
3	0.1 eq., no UV	141.1 (As)	41.7 (As) 44.9 (As_2O_3)	–[b]	–[c]
4	Gray As (blank)	–[a]	41.7 (As) 44.8 (As_2O_3	–[b]	–[c]

[a]Not measured
[b]Not detected in significant amount
[c]No complex observed

sample was excluded based on the Raman spectra (see Supplementary Fig. S6 in Supporting Information). The attached ligands were mainly CO groups, as is evident from the oxygen 1s spectrum with a peak at 531.7 eV (Supplementary Fig. S7A) and the carbon 1s spectrum, with a shift of 285.4 eV. The presence of the MeCN group as a ligand on chromium was confirmed by the peak at 283.4 eV (Supplementary Fig. S7B). The main arsenic and chromium XPS peaks are listed in Table 2 for comparison. The main difference between the experiments with 1.5 and 0.1 eq. of $Cr(CO)_6$ is the formation of different complexes. In the case of 0.1 eq., shown as entry 2, the ratio between As $3p_{3/2}$ peaks was almost 5:1, while in the case of 1.5 eq, shown as entry 1, the ratio was almost 1:1; these results suggest the formation of two complexes with a similar concentration and the general formula mentioned above and support the conclusion based on the FTIR spectra. Both complexes were clearly different from pure arsenic (entry 4) or arsenic after treatment with Cr $(CO)_6$ without UV irradiation (entry 3), which both show peaks only at 41.7 eV (As $3d_{5/2}$) and 141.1 eV (As $3p_{3/2}$, entry 3), and chromium was not detected.

Conclusion

In conclusion, we demonstrated photoassisted exfoliation of gray arsenic and its modification with chromium hexacarbonyl. The prepared materials represent the first covalently modified gray arsenic materials and offer possibilities for further derivatization, for example, by the addition of organometallic compounds to carbonyl functional groups, the exchange of remaining carbonyl ligands by aromatic compounds, or the development of few-/single-layer pnictogen coordination chemistry, with possible application as catalysts for mild oxidation or metathesis reactions. In addition, our approach enables the synthesis of arsenic complexes with different metals where the scope of reactions is even broader, such as for hydrogenation reactions with platinum or palladium or cross-coupling reactions, like Suzuki coupling.

Acknowledgements
M. P. acknowledges the financial support of the Grant Agency of the Czech Republic (EXPRO: 19-26896X). J. S. greatly acknowledges the financial support of the Grant Agency of the Czech Republic (GACR No. 19−17593Y) and the access to computational resources, which were supplied by the Ministry of Education, Youth and Sports of the Czech Republic under the Projects CESNET (Project No. LM2015042) and CERIT-Scientific Cloud (Project No. LM2015085) provided within the program Projects of Large Research, Development and Innovations Infrastructures. This research has also been financially supported by the Ministry of Education, Youth and Sports of the Czech Republic under the Project CEITEC 2020 (LQ1601). This study was performed with the financial support of the Neuron Foundation for science support.

Author details
[1]Department of Inorganic Chemistry, University of Chemistry and Technology Prague, Technicka 5, 166 28 Prague 6, Czech Republic. [2]Department of Chemical and Biomolecular Engineering, Yonsei University, 50 Yonsei-ro, Seodaemun-gu, Seoul 03722, Korea. [3]Future Energy and Innovation Laboratory, Central European Institute of Technology, Brno University of Technology, Purkyňova 656/123, CZ-616 00 Brno, Czech Republic

Conflict of interest
The authors declare that they have no conflict of interest.

Supplementary information is available for this paper at https://doi.org/10.1038/s41427-019-0142-x.

Received: 21 January 2019 Revised: 22 April 2019 Accepted: 4 May 2019.
Published online: 23 August 2019

References

1. Khan, A. H. et al. Two-dimensional (2D) nanomaterials towards electrochemical nanoarchitectonics in energy-related applications. *Bull. Chem. Soc. Jpn.* **90**, 627–648 (2017).
2. Lee, M. J. et al. Synaptic devices based on two-dimensional layered single-crystal chromium thiophosphate (CrPS4). *NPG Asia Mater.* **10**, 23–30 (2018).
3. Chia, X. & Pumera, M. Characteristics and performance of two-dimensional materials for electrocatalysis. *Nat. Catal.* **1**, 909–921 (2018).
4. Maeda, K. & Mallouk, T. E. Two-dimensional metal oxide nanosheets as building blocks for artificial photosynthetic assemblies. *Bull. Chem. Soc. Jpn.* **92**, 38–54 (2019).
5. Abellán, G. et al. Noncovalent functionalization of black phosphorus. *Angew. Chem. Int. Ed.* **55**, 14557–14562 (2016).
6. Marcia, M., Hirsch, A. & Hauke, F. Perylene-based non-covalent functionalization of 2D materials. *FlatChem* **1**, 89–103 (2017).
7. Shi, M. et al. Donor–acceptor type blends composed of black phosphorus and C60 for solid-state optical limiters. *Chem. Commun.* **54**, 366–369 (2018).
8. Vishnoi, P. et al. Doping phosphorene with holes and electrons through molecular charge transfer. *ChemPhysChem* **18**, 2985–2989 (2017).
9. Abellán, G. et al. Fundamental Insights into the degradation and stabilization of thin layer black phosphorus. *J. Am. Chem. Soc.* **139**, 10432–10440 (2017).
10. Kang, J. et al. Stable aqueous dispersions of optically and electronically active phosphorene. *Proc. Natl. Acad. Sci. USA.* **113**, 11688–11693 (2016).

11. Matthews, P. D. et al. Black phosphorus with near-superhydrophobic properties and long-term stability in aqueous media. *Chem. Commun.* **54**, 3831–3834 (2018).
12. Abellán, G. et al. Noncovalent functionalization and charge transfer in antimonene. *Angew. Chem. Int. Ed.* **56**, 14389–14394 (2017).
13. Tao, W. et al. Antimonene quantum dots: synthesis and application as near-infrared photothermal agents for effective cancer therapy. *Angew. Chem. Int. Ed.* **56**, 11896–11900 (2017).
14. Gusmão, R., Sofer, Z. & Pumera, M. Functional protection of exfoliated black phosphorus by noncovalent modification with anthraquinone. *ACS Nano* **12**, 5666–5673 (2018).
15. Ryder, C. R. et al. Covalent functionalization and passivation of exfoliated black phosphorus via aryl diazonium chemistry. *Nat. Chem.* **8**, 597 (2016).
16. Guo, W., Song, H. & Yan, S. Stable black phosphorus quantum dots for alkali PH sensor. *Opt. Commun.* **406**, 91–94 (2018).
17. Zhao, Y. et al. Stable and multifunctional dye-modified black phosphorus nanosheets for near-infrared imaging-guided photothermal therapy. *Chem. Mater.* **29**, 7131–7139 (2017).
18. Giannozzi, P. et al. Advanced capabilities for materials modelling with quantum ESPRESSO. *J. Phys: Condens. Matter* **29**, 465901 (2017).
19. Grim, S. O., Del Gaudio, J., Molenda, R. P., Tolman, C. A. & Jesson, J. P. Unsymmetrical bis-phosphorus ligands. V. Group VI metal carbonyl derivatives. *J. Am. Chem. Soc.* **96**, 3416–3422 (1974).
20. Chen, M. et al. Organometallic chemistry of graphene: photochemical complexation of graphene with group 6 transition metals. *Carbon* **129**, 450–455 (2018).
21. Sarkar, S., Niyogi, S., Bekyarova, E. & Haddon, R. C. Organometallic chemistry of extended periodic π-electron systems: hexahapto-chromium complexes of graphene and single-walled carbon nanotubes. *Chem. Sci.* **2**, 1326–1333 (2011).
22. Strohmeier, W. Photochemical substitutions on metal carbonyls and their derivatives. *Angew. Chem., Int. Ed. Engl.* **3**, 730–737 (1964).
23. Ross, B. L., Grasselli, J. G., Ritchey, W. M. & Kaesz, H. D. Spectroscopic studies of the complexes of acrylonitrile and acetonitrile with the carbonyls of chromium, molybdenum, and tungsten. *Inorg. Chem.* **2**, 1023–1030 (1963).
24. Tsai, H.-S. et al. Direct synthesis and practical bandgap estimation of multilayer arsenene nanoribbons. *Chem. Mater.* **28**, 425–429 (2016).
25. Fillman, L. M. & Tang, S. C. Thermal decomposition of metal carbonyls: a thermogravimetry-mass spectrometry study. *Thermochim. Acta* **75**, 71–84 (1984).